# Magnetic Field Effect to Relative *K* X-ray Intensity Ratios of Light Lanthanides

M. Uğurlu*

Atatürk University, Faculty of Sciences, Department of Physics, Erzurum 25240, Turkey

*(Received August 21, 2019; revised version September 10, 2019; in final form October 3, 2019)*

La, Ce, Pr, Nd, Sm, and Eu elements were used in order to determine variation of $K_\beta$ to $K_\alpha$ X-ray intensity ratios at the magnetic field ($B$= 0, 0.4, 0.8 T). The samples were irritated by 59.54 keV $\gamma$-rays from $^{241}$Am radioactive point source via energy dispersive X-ray fluorescence spectroscopy. $K$ X-rays emitted by samples were counted with a high resolution Si(Li) solid-state detector. The experimental results were compared with the literature. The analysis shows that $K_\beta$ to $K_\alpha$ X-ray intensity ratios of the elements without magnetic field are compatible with the past studies and although $K_\beta$ and $K_\alpha$ peak intensities change with variation of the magnetic field, the intensity ratios do not change.

DOI: 10.12693/APhysPolA.136.983

PACS/topics: magnetic field, X-ray intensity ratios, light lanthanides

## 1. Introduction

The lanthanides may be broadly classified into two groups: the "light" (or the cerium) group consists of La, Ce, Pr, Nd, Sm, Eu, and Gd, and the "heavy" (or the yttrium) consists of Y, Tb, Dy, Ho, Er, Tm, Yb, and Lu elements. The term "light" and "heavy" are derived from the fact that "light" materials are generally more soluble than "heavy" ones in a given solvent system used for separation. Electronic ground configuration of lanthanide atoms are [Xe] $4f^n6s^2$ (with the exception that ground configuration of La, Ce, Gd, Lu is [Xe] $4f^n5d^16s^2$).

If an atom is bombarded with different particles which have enough energy for the ionization, the shell electron is ejected from the atom and a vacancy occurs. The electron transitions are carried out from upper shells to fill the vacancy. During this process, an X-ray emission (radiative) or the Auger transition (non-radiative) happen. For instance, if an electron is ejected from $K$ shell, $K_{\alpha_1}$, $K_{\alpha_2}$, $K_{\beta_1}$ or $K_{\beta_2}$ X-ray fluorescence can be emitted. In the emission of $K_{\alpha_1}$, the vacancy occurs in the $L_3$ subshell. If this vacancy is filled with an $M_1$ electron, $M_5$ electron is ejected (the Auger transition) by X-ray emitted. Then the new vacancy occurs in $M_1$ shell. $M_5$ electron fills the vacancy. During this case, $N_5$ electron is ejected (the Coster–Kronig transition) by X-ray emission. The $N_3$ electron fills in $M_5$ vacancy and $N_5$ electron is ejected (the Auger transition), etc. This case goes on until all transitions are finished. Finally, the remaining vacancy is filled by a free electron in an outer shell. The transitions occur by depending on quantum mechanical selection rules ($\Delta j = \pm 1$, $\Delta l = \pm 1$ and $\Delta n \neq 0$, where $j$, $l$, and $n$ are the quantum numbers) [1].

The Le Chatelier–Braun principle is defined that when a system in equilibrium is applied by external factors (such as pressure, volume, magnetic field, electric field, temperature, and concentration), it will try to relieve the stress and adapt a new equilibrium. In the absence of the magnetic field, the valence states are doubly degenerate. The degeneration disappears in the presence of the magnetic field. Under the external magnetic field, the atoms of which the orbital magnetic moments are of the same direction with the external magnetic field try to reduce effect of field by decreasing orbital magnetic moments. So the angular velocity of electrons decreases. The atoms of which the orbital magnetic moments are in the opposite direction with the external magnetic field try to reduce effect of field by increasing orbital magnetic moments. So the angular velocity of electrons increases. Consequently, the decreasing or increasing electron velocity is possible for delocalization of electron.

Three types of electronic transitions can occur for lanthanide and actinide systems. These are: $f \rightarrow f$ transitions, $nf \rightarrow (n+1)d$ transitions, and ligand $\rightarrow$ metal $f$ charge transfer transitions [2]. The lanthanide atoms have partly filled $4f$ subshell. If the atom is excited by magnetic dipole and electric dipole radiation of the $f$–$f$ transitions occurs [3]. In the atom induced by an external magnetic field $f$–$f$ exchange interactions happen and this state causes the intrinsic magnetism [4].

X-ray intensity ratios are used to explain the interaction of matter with X-rays and are characteristic values for each element. A lot of study have been performed to $K_\beta$ to $K_\alpha$ X-ray intensity ratios $R$ values of elements, compounds and alloys with magnetic field and without magnetic field [5–15]. $R$ depends on the physical and chemical environments of the element [16], the structure of chemical bonding, the individual characteristics of the structure of molecules, complexes, and crystals (polarity, valency and electronegativity of atoms, coordination number, ionicities of covalent bond, etc.) [17].

*e-mail: ugurlumine25@gmail.com

$R$ is a sensitive parameter to find the variations in the valence electronic structure of $3d$ transition elements [8]. $R$ is dependent on the electronic configuration of the atom that emits X rays and influenced by chemical environments [18]. The present study is focused on the changing of the relative $R$ values of La, Ce, Pr, Nd, Sm, Eu in pure form under the external magnetic field.

## 2. Experimental procedure

La, Ce, Pr, Nd, Sm, and Eu samples (in powder form) were acquired and applied with $\approx$ 1 GPa pressure to transform foil form (shape of circle and with $\approx$ 13 mm diameter). The mass thickness, sample thickness, and density properties of the elements are given in Table I. After ensuring the stability of the detector, the distance between the center of the radioactive source and the sample was set to 7.74 cm. The distance between the center of the sample and Be window (12.5 $\mu$m) of the detector was set to 3.7 cm. In addition, to obtain the maximum count and to reduce the scattering radiation intensity, the angle of the filament wire (sample attached to this wire) on the Al sample holder to the horizontal plane (angle between sample-radioactive source plane ($\theta_1$) and angle between sample-detector plane ($\theta_2$)) were fixed at 45°. The distance between the magnets of the electromagnet was 1.44 cm to ensure the stability of the sample between the electromagnets and the smooth magnetic field. All these values were kept constant throughout the experiment. The elements were mounted in the middle of the sample holder, which was placed between electromagnets producing the magnetic field $\approx$ 2.8 T. In this study, applied magnetic field values were 0.4 and 0.8 T. The stability of these values was enabled by an ampere meters during the experiment. The samples were excited with 59.54 keV $\gamma$-rays from a $^{241}$Am radioactive point source. The radiation emitted from the elements was detected via Si(Li) solid state detector. The data were collected into 4096 channels of a digital spectrum analyzer DSA-1000.

TABLE I

The mass thickness, sample thickness and density properties of the elements.

| Elements | Mass [g] | Sample thickness [cm] | Mass thickness [g/cm$^2$] | Density of the pressed powder [g/cm$^3$] | Density of the solid samples [g/ cm$^3$] |
|---|---|---|---|---|---|
| La | 0.42488 | 0.1 | 0.32010 | 3.2010 | 6.15 |
| Ce | 0.30561 | 0.09 | 0.23024 | 2.5583 | 6.69 |
| Pr | 0.22437 | 0.09 | 0.17436 | 1.9374 | 6.71 |
| Nd | 0.67044 | 0.09 | 0.512097 | 5.6996 | 7.00 |
| Sm | 0.32685 | 0.1 | 0.24625 | 2.4625 | 7.47 |
| Eu | 0.13388 | 0.04 | 0.10404 | 2.6010 | 5.24 |

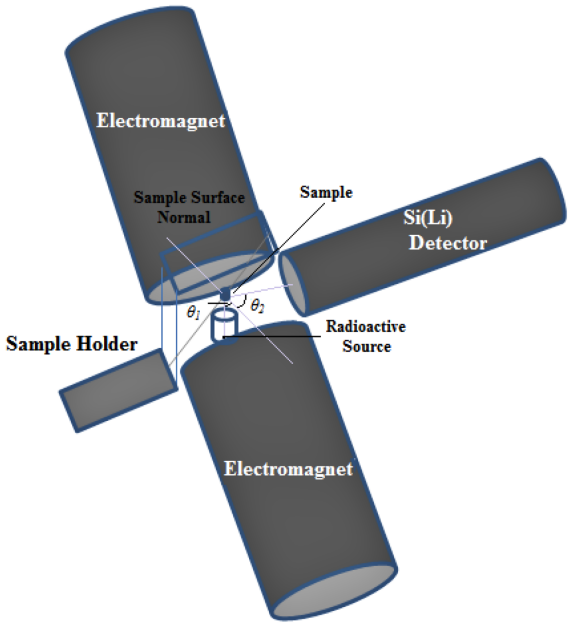


Fig. 1. Experimental geometry.

The experimental geometry that consists of electromagnets, Si(Li) detector, $^{241}$Am radioactive point source and sample holder is given in Fig. 1. The calibrating of the detector was given previous study [15].

The experimental $R$ values were calculated by the following equation

$$R = \frac{I_{K_\beta}}{I_{K_\alpha}} = \frac{N_{K_\beta}}{N_{K_\alpha}} \frac{\beta_{K_\alpha}}{\beta_{K_\beta}} \frac{\varepsilon_{K_\alpha}}{\varepsilon_{K_\beta}}, \tag{1}$$

where $N_{K_i}$ represents the number of counts under the $K_i$ peaks, $\beta_{K_i}$ is the self-absorption correction factor for incident photons and characteristic X-rays emitted. It is defined as

$$\beta_{K_i} = \frac{1 - \exp\left(-t\left[\frac{(\mu/\rho)_i}{\cos\theta_1} + \frac{(\mu/\rho)_e}{\cos\theta_2}\right]\right)}{t\left[\frac{(\mu/\rho)_i}{\cos\theta_1} + \frac{(\mu/\rho)_e}{\cos\theta_2}\right]}, \tag{2}$$

where $(\mu/\rho)_i$ and $(\mu/\rho)_e$ are the mass attenuation coefficients (cm$^2$/g) of incident photons and emitted characteristic X-rays. The values are obtained by means of WinXCom [19, 20]. The angle between incident $\gamma$ rays and the target normal determines $\theta_1$, while between emitted X-rays and the target normal—$\theta_2$. The target mass thickness is $t$ (g/cm$^2$).

The ratio $\varepsilon_{K\alpha}/\varepsilon_{K\beta}$ was obtained by using the following formula

$$I_0 G \varepsilon_{K_i} = \frac{N_{K_i}}{\sigma_{K_i}} \beta_{K_i} t_i. \tag{3}$$

Here, $I_0 G\varepsilon$ is called photon flux and consists of $I_0$ (intensity of stimulating photon), $G$ (geometry factor), and $\varepsilon$ (detector efficiency). In above formula, $N_{K_i}$ is the net number of counts under corresponding peak, $\sigma_{K_i}$ is the fluorescence cross-section at energy value interested in. The calculation of $I_0$, $G$, and $\varepsilon_{K_i}$ one by

one is very hard. However, $I_0 G\varepsilon_{K_i}$ can be determined with the pure elements whose X-ray energy values are in energy location investigated. Under the same experimental conditions, $K$ X-ray spectra of pure elements are obtained. $I_0 G\varepsilon_{K_i}$ for any energy can be obtained by using peak areas. These values are plotted as a function of energy. $I_0 G\varepsilon_{K_i}$ for $K_\alpha$ vs. $K_\beta$ X-rays can be calculated by the help of this function.

All parts of the system were stable during the experiment and the measurements repeated with every sample, without sample, with magnetic field, and without magnetic field for determining the experimental errors.

## 3. Results and discussion

The typical $K$ X-ray spectra of La without magnetic field are given in Fig. 2. The change of $K_\beta$ and $K_\alpha$ peak areas ($N_{K_i}$) with magnetic field is given in Fig. 3.

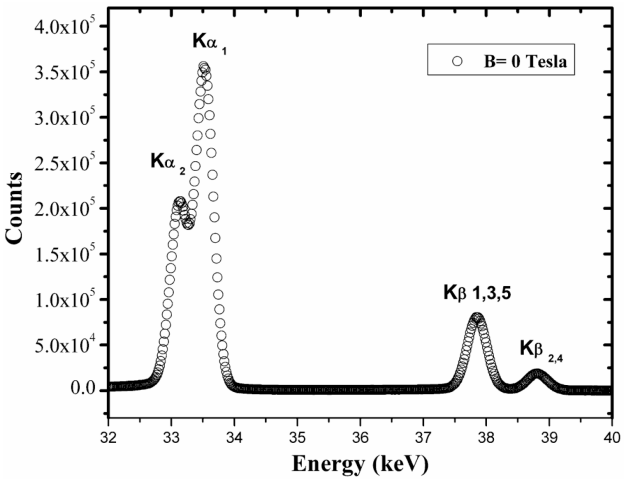


Fig. 2. The changing of $K_\alpha$ and $K_\beta$ X-ray intensity of La without the magnetic field.

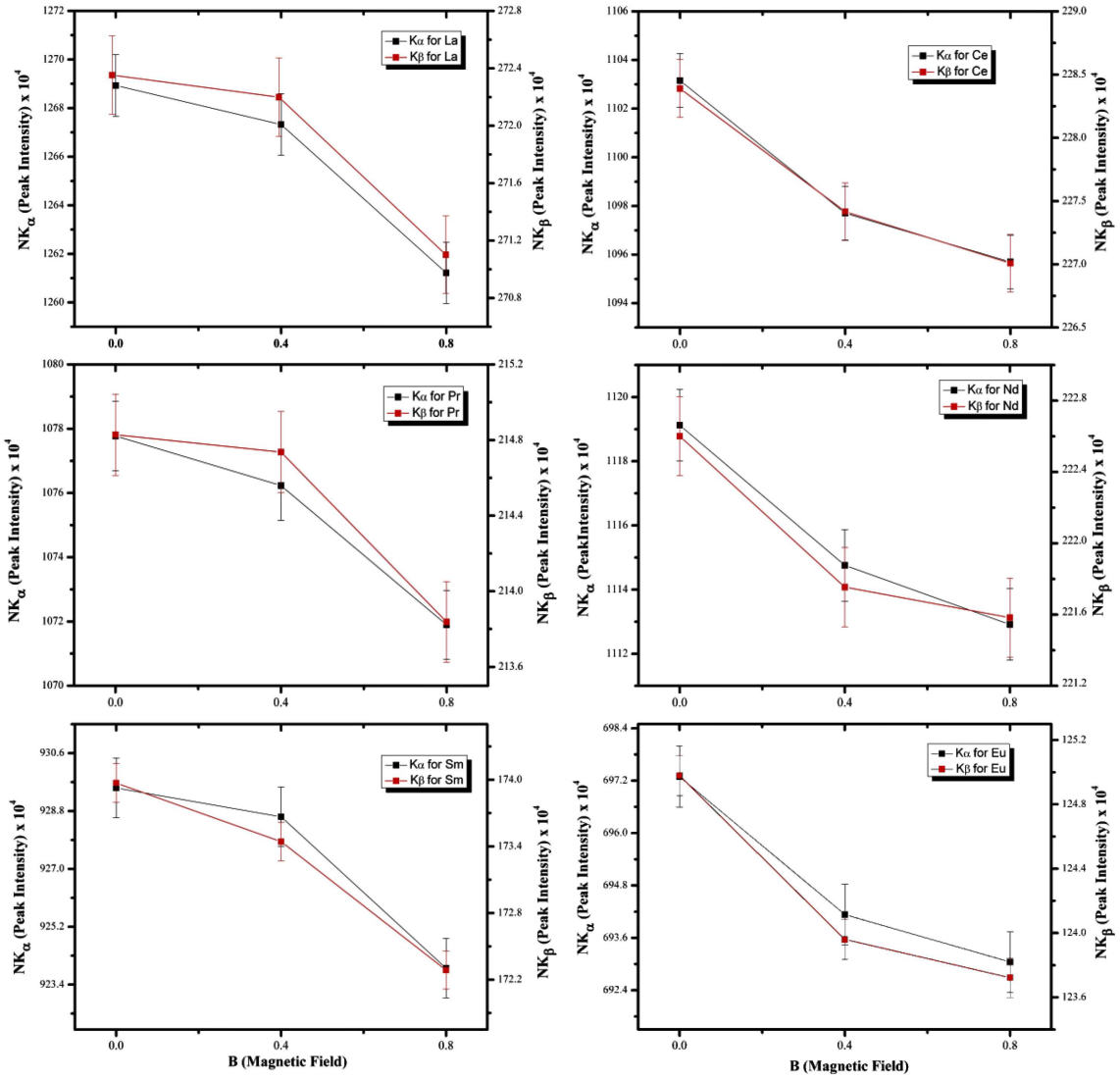


Fig. 3. The variation of $K_\alpha$ and $K_\beta$ X-ray peak intensities for samples with the magnetic field.

TABLE II

The experimental values of $R = I_{K_\beta}/I_{K_\alpha}$ X-ray intensity ratios of samples La, Ce , Pr, Nd, Sm and Eu at $B = 0$, 0.4, 0.8 T.

| | $B = 0$ T | $B = 0.4$ T | $B = 0.8$ T | Ref. [1] | Ref. [2] | Ref. [3] | Ref. [4] |
|---|---|---|---|---|---|---|---|
| La | $0.232 \pm 0.005$ | $0.233 \pm 0.005$ | $0.233 \pm 0.005$ | 0.2347 | 0.2040 | 0.2304 | 0.2430 |
| Ce | $0.234 \pm 0.005$ | $0.234 \pm 0.005$ | $0.234 \pm 0.006$ | 0.2488 | 0.2480 | 0.2316 | 0.2440 |
| Pr | $0.236 \pm 0.006$ | $0.236 \pm 0.006$ | $0.236 \pm 0.006$ | 0.2475 | – | 0.2336 | 0.2447 |
| Nd | $0.244 \pm 0.006$ | $0.244 \pm 0.006$ | $0.244 \pm 0.006$ | 0.2415 | 0.2470 | 0.2354 | 0.2480 |
| Sm | $0.253 \pm 0.005$ | $0.254 \pm 0.005$ | $0.253 \pm 0.005$ | – | 0.2500 | 0.2389 | 0.2510 |
| Eu | $0.260 \pm 0.004$ | $0.260 \pm 0.004$ | $0.260 \pm 0.004$ | – | – | 0.2405 | 0.2540 |

It is seen that $K_\beta$ and $K_\alpha$ peak areas ($N_{K_i}$) of the elements studied decrease by increasing magnetic field. Demir and Şahin (2007) have investigated $K$-shell X-ray production cross-sections and $K$ to $L$ and $M$-shell radiative vacancy transfer probabilities for Nd, Eu, Gd, Dy, and Ho at excitation with 59.5 keV photons in an external magnetic field. They have found that while $K_{\alpha_1}$, $K_{\beta_1'}$ and $K_{\beta_2'}$ X-ray production cross-sections increase in the external magnetic field, $K_{\alpha_2}$ X-ray production cross-sections do not change in the external magnetic field. They have explained the cause of this situation with the alignment of the inner shell vacancy in ions (this result may be sourced from both the final and initial states of the X-ray transitions may have an aligned vacancy if the angular momenta of the states are larger than 1/2 in the ionization of an inner atomic electron by radiation.) [21].

The experimental $R$ values of La, Ce, Pr, Nd, Sm, and Eu metals in pure form under external magnetic field are shown in Table II. As seen in Table II, the calculated $R$ values of La, Ce, Pr, Nd, Sm, and Eu without magnetic field are in agreement with the previous studies (Ref. 1 [22], Ref. 2 [23], Ref. 3 [24], and Ref. 4 [25]). No other theoretical and experimental data are available for comparison with the results calculated by this study for $B \neq 0$. However, the obtained $R$ values for the lanthanide elements studied are stable with the magnetic field increasing. That is arisen from decrease of $N_{K_i}$.

Also, as the atomic number increases, the calculated $R$ values of light lanthanides increase and results are given in Table II and Fig. 4. Polasik (1998) has studied influence of changes in the valence electronic configuration on the $K_\beta$ to $K_\alpha$ X-ray intensity ratios of the $3d$ transition metals. It has been obtained that $K_\beta$ to $K_\alpha$ X-ray intensity ratios of the $3d$ transition metals depend on the valence electronic configurations and this value increase with increase in the atomic number of elements [5]. Yilmaz (2017) studied $K_\beta/K_\alpha$ X-ray intensity ratios for some elements in the atomic number range $28 < Z < 39$ at 16.896 keV. He obtained that $K_\beta/K_\alpha$ intensity ratio is also larger than smaller atomic number elements [26]. In [1–4] it was found that $R$ values increase with increase in atomic number. Therefore, $R$ values do not change with the increase in the magnetic field in this study.

As mentioned in the introduction section, under the magnetic field, internal structure of the atom is broken. Some unpaired electrons try to transfer different

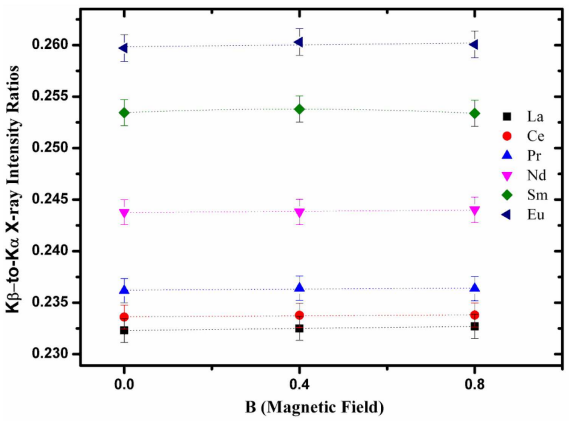


Fig. 4. The variation of $K_\beta$ to $K_\alpha$ X-ray intensity ratios for light lanthanides with the magnetic field.

place to have extra energy or some try to loose energy. If the electrons' energy in the external magnetic field is high enough, the electrons may go out of the atom, to other atoms, other shells, other orbitals, or different energy level of the same orbital in the external magnetic field. This situation affects radiation of an atom.

The $K_\beta$ and $K_\alpha$ X-rays are supplied for internal transitions of the atom. The meaning of the decrease of peak intensity values with increase of external magnetic field may be attributed to the transition of unpaired electrons at the atomic levels in the magnetic field. There are electron transitions between $4f$ states and $4f$–$5d$ states of an atom and of individual metal atoms. The $d$-DOS (density of states) and $f$-DOS are closely aligned, a signature of the expected $4f$–$5d$ hybridization common in lanthanide materials [27].

## 4. Conclusions

When these results are analysed, some conclusions can be reached. Firstly, it was seen that $K_i$ peak areas decrease by increasing the magnetic field. Secondly, the experimental data indicates that $R$ values for light lanthanides were also found distinct from each other. As the atomic number of these elements increase, $R$ values increase. This is convenient to literature and theoretical results. Thirdly, the $R$ values do not change with increasing magnetic field.

## References


[1] F. Akman, *Appl. Radiat. Isot.* **115**, 295 (2016).

[2] H.C. Aspinall, *Chemistry of the f Block Elements*, University of Liverpool, Liverpool 2001.

[3] S. Cotton, *Lanthanides and Actinides Chemist*, Oxford University Press, Oxford 1991.

[4] J.L.F. Da Silva, *Theory of Lanthanide Systems: Valence Transitions and Interplay of Kondo Effect and Disorder*, Condensed Matter Université Grenoble Alpes, 2016.

[5] M. Polasik, *Phys. Rev. A* **58**, 1840 (1998).

[6] S. Raj, B. Dhal, H.C. Padhi, M. Polasik, *Phys. Rev. B* **58**, 9025 (1998).

[7] S. Raj, H.C. Padhi, M. Polasik, F. Pawlowski, D.K. Basa, *Solid State Commun.* **116**, 563 (2000).

[8] S. Raj, H.C. Padhi, M. Polasik, F. Pawlowski, D.K. Basa, *Phys. Rev. B* **63**, 073109 (2001).

[9] D. Demir, Y. Şahin, *Eur. J. Phys. D* **42**, 211 (2007).

[10] S. Porikli, Y. Kurucu, *Appl. Radiat. Isot.* **66**, 1381 (2008).

[11] I. Han, L. Demir, *Phys. Rev. A* **80**, 052503 (2009).

[12] I. Han, L. Demir, *Appl. Radiat. Isot.* **68**, 1035 (2010).

[13] B. Alım, I. Han, L. Demir, *Appl. Radiat. Isot.* **112**, 5 (2016).

[14] U. Perişanoğlu, B. Alım, M. Uğurlu, L. Demir, *Appl. Radiat. Isot.* **115**, 183 (2016).

[15] M. Uğurlu, B. Alım, I. Han, L. Demir, *J. Alloys Comp.* **695**, 2619 (2017).

[16] S. Raj, H.C. Padhi, M. Polasik, D.K. Basa, *Solid State Commun.* **110**, 275 (1999).

[17] S. Porikli, İ. Han, P. Yalçin, Y. Kurucu, *Spectrosc. Lett.* **4**, 38 (2011).

[18] I. Yamoto, H. Kaji, K. Yoshihara, *J. Chem. Phys.* **84**, 522 (1986).

[19] L. Gerward, N. Guilbert, K.B. Jensen, H. Levring, *Radiat. Phys. Chem.* **60**, 23 (2001).

[20] L. Gerward, N. Guilbert, K.B. Jensen, H. Levring, *Radiat. Phys. Chem.* **71**, 653 (2004).

[21] D. Demir, Y. Şahin, *X-Ray Spectrom.* **36**, 178 (2007).

[22] V.D. Mistry, C.A. Quarles, *Phys. Lett. A* **36**, 221 (1971).

[23] S.I. Salem, S.L. Panossıan, R.A. Krause, *At. Data Nucl. Data Tables* **14**, 91 (1974).

[24] J.H. Scofield, *At. Data Nucl. Data Tables* **14**, 121 (1974).

[25] M. Ertuğrul, Ö. Söğüt, Ö. Şimşek, E. Büyükkasap, *J. Phys. B At. Mol. Opt. Phys.* **34**, 909 (2001).

[26] R. Yilmaz, *J. Radiat. Res. Appl. Sci.* **10**, 172 (2017).

[27] J.I. Pacold, Ph.D. Thesis, University of Washington, 2014.